



An Electrochemical Deposition Route for Obtaining α -Fe₂O₃ Thin Films

II. EQCM Study and Semiconductor Properties

Ricardo Schreiber,^a Cynthia Llewelyn,^a Francisca Vera,^a Paula Cury,^a
Eduardo Muñoz,^a Rodrigo del Río,^b Humberto Gómez Meier,^a
Ricardo Córdova,^{a,*} and Enrique A. Dalchiele^{c,*z}

^aInstituto de Química, Facultad de Ciencias, Pontificia Universidad Católica de Valparaíso, Valparaíso, Chile

^bDepartamento de Química Inorgánica, Facultad de Química, Pontificia Universidad Católica de Chile, San Joaquín, Santiago, Chile

^cInstituto de Física, Facultad de Ingeniería, 11000 Montevideo, Uruguay

The electrochemical formation of hematite (α -Fe₂O₃) precursor thin films (oxyhydroxide iron compounds), onto gold substrates in an aqueous solution of Fe(III) + KF + H₂O₂ was investigated in situ using an electrochemical quartz crystal microbalance (EQCM) and voltammetric techniques. Nanostructured α -Fe₂O₃ obtained after annealing of oxyhydroxide iron compounds thin films have been prepared onto SnO₂/F covered glass substrates through a potential cycling procedure in this electrolytic bath. Photoelectrochemical measurements, carried out in 0.1 M NaOH + 0.05 M KI electrolyte at pH 13, show an n-type behavior, a flatband potential of -1.08 V vs saturated mercury/mercury sulfate reference electrode, and an apparent donor density of $1.26 \times 10^{19} \text{ cm}^{-3}$ at 1 kHz.

© 2007 The Electrochemical Society. [DOI: 10.1149/1.2756160] All rights reserved.

Manuscript submitted February 8, 2007; revised manuscript received June 12, 2007. Available electronically July 18, 2007.

Iron oxide α -Fe₂O₃ (hematite) is an attractive semiconductor material for photoelectrochemical and photocatalytic purposes due to its stability, abundance, and environmental compatibility, as well as its suitable bandgap and valence bandedge position.¹⁻¹⁰ In general, hematite exhibits a n-type character, which can be due to the tendency of α -Fe₂O₃ to become oxygen deficient, irrespective of the preparation method.

Unfortunately, in spite of the merits stated above, because of the weak optical absorption coefficient, small carrier mobility, short hole diffusion length, and low rate constant of water oxidation by surface trapped holes, illuminated hematite electrodes normally show poor efficiency as photoanodes in water oxidation.^{d 10-12} However, recent studies have indicated that nanocrystalline morphology^e could be one way to overcome those limitations and increase the photon-to-current yield by minimizing the distance the minority carriers have to diffuse before reaching the interface.^{5,11,14,15} Additionally, exhibiting large internal surface areas is an inherent property of nanostructured semiconductor thin films of main importance in photoelectrochemical devices.

Various techniques have been investigated for the synthesis of hematite nanocrystalline thin films: thermal evaporation,¹⁶ aqueous chemical growth,¹⁶ spray-pyrolysis,^{8,14,17} ultrasonic spray-pyrolysis,¹⁷ and the sol-gel method.¹⁸ Electrodeposition is a technique that is well-suited to the preparation of nanostructures.¹⁹ In fact, through proper parameter control, electrodeposited materials from nanostructured to even epitaxial films with better-quality properties can also be achieved.^{20,21} Moreover, the electrodeposition technique is now emerging as an important low-cost and low-temperature method for preparing semiconducting thin films.²² In the last years several reports have appeared concerning the electrodeposition of iron oxide thin films onto foreign substrates: Fe₃O₄ (magnetite), α -FeOOH (goethite), and γ -FeOOH (lepidocrocite).²³

However, in spite of this, to the best of our knowledge after the pioneering work of Zotti et al. in 1998²⁴ and the first part of this work,²⁵ there are no recent papers reporting the electrodeposition of hematite thin films. In our previous study, the growth of hematite nanocrystalline thin films by a new electrochemical method through a potential cycling procedure has been reported.²⁵ So, the present work is part of our continuation of studies on the preparation and characterization of pure-phase hematite thin films.

This work reports a study of the electrochemical growth process of α -Fe₂O₃ onto fluorine-doped tin oxide (FTO) by means of cyclic voltammetry and onto polycrystalline gold electrodes by means of electrochemical quartz crystal microbalance (EQCM). The benefit of the combined use of massograms and voltammograms for the study of different types of electrochemical processes has been reported by several authors.²⁶ The present study also includes a photoelectrochemical characterization of the hematite thin films with liquid junctions which provides information on (i) photoactivity and (ii) the optoelectronic properties of the semiconductor thin films (e.g., flatband potential and doping density). The last are very important factors that might be correlated with complete solar-cell performance.²⁷

Experimental

Iron oxide thin films have been electrochemically grown by potential cycling onto transparent electrode substrates consisting of glass plates with a conductive thin film of FTO on one side (Nippon Sheets, sheet resistance of about 10–30 Ω/\square). A typical three-electrode electrochemical cell geometry has been used, comprising a FTO substrate (1.7 cm²), a Pt wire, and a saturated mercury/mercury sulfate (SMSE), $E = 0.650 \text{ V}$, vs normal hydrogen electrode (NHE)] as working, counter, and reference electrodes, respectively. The electrodeposition bath consisted of an aqueous solution of 5 mM FeCl₃ + 5 mM KF + 1 M H₂O₂ + 0.1 M KCl. All solutions were prepared from analytical-grade reagents and 18.3 M Ω cm Millipore water. The electrodeposition was performed at 50°C. Argon was flushed through the cell and the electrolyte prior to the experiments, and an argon flow was maintained over the solution during measurements and electrodeposition process. In order to study the electrochemical mechanism of the iron oxide deposition, cyclic voltammetry analysis was done using an Au/quartz electrode. Electrochemical growth was done by a potential cycling procedure at a potential sweep rate of 0.02 V/s, from 0.0 to -0.9 vs SMSE, for a whole of 50 cycles. The thickness of the obtained iron

* Electrochemical Society Active Member.

^z E-mail: dalchiel@fing.edu.uy

^d An electron mobility less than 10^{-2} – $10^{-1} \text{ cm}^2 \text{ V}^{-1} \text{ s}^{-1}$ has been reported and a diffusion length of holes to only 2–4 nm has been stated, which is 100 times lower than many other (III-V) oxides.

^e Nanocrystalline materials are those formed by polycrystals with grain sizes of the order of nanometers (nanograins), grain size $\leq 100 \text{ nm}$, i.e., is a system in which at least one dimension is $\leq 100 \text{ nm}$ (typically including layerlike, wirelike, and particle-like structures).¹³

oxide films was about 1 μm for all the samples. The electrochemical measurements and electrodepositions were carried out using a Zanker IM6e potentiostat/galvanostat and an EQCM Maxtek model RQCM coupled to a Pine RDE 4 potentiostat. The iron oxide thin films were annealed in air for 20 min at 500°C in a Blue M model Lindberg tube furnace. The electrochemical impedance spectroscopy measurements were done by applying a sinusoidal perturbation of 10 mV at different frequencies ($f = 0.1, 0.5, \text{ and } 1.0 \text{ kHz}$) in a 0.1 M NaOH. The photoelectrochemical measurements were performed in a three-electrode glass cell. The working hematite thin-film electrode had a surface of ca. 1 cm^2 , and a Pt wire and a SMSE were used as the counter and the reference electrodes, respectively. A xenon lamp of 75 W (Oriental Instruments 6263) mounted in a lamp holder (Oriental 66902) was connected to the cell through a water filter (Oriental 61945) and a 1 m length optical fiber (Oriental 77578). A power supply of 40–200 W (Oriental 68907) was used to generate the arc in the lamp. The illumination power was quantified inside the cell by means of an energy radiant meter (Oriental 70260). A pure argon stream was passed through the solution for 30 min before measurements and over the solution when the experiments were under way. The electrolyte solution used for photoelectrochemical measurements was 0.1 M NaOH + 0.05 M KI solution at pH 13.

Results and Discussion

Growth process and electrochemical preparation of $\alpha\text{-Fe}_2\text{O}_3$ thin films.—As was previously reported in our earlier paper, the synthesis of the $\alpha\text{-Fe}_2\text{O}_3$ thin films was done using a novel electrochemical route through a potential cycling procedure in a suitable electrolyte.²⁵ A voltammetric experiment was performed between 0.0 and -0.9 V , where only the hydrogen peroxide reduction can be observed. After 25 potential cycles, a red film covering the electrode surface was observed. The X-ray diffraction (XRD) measurements showed that the as-electrodeposited iron oxide films were either amorphous or a very small crystallite size, which normally occurs when metal oxides are formed at relatively low temperatures.²⁵ When the films are annealed at 520°C for 30 min, XRD analysis confirms the presence of the $\alpha\text{-Fe}_2\text{O}_3$ phase.²⁵ This is an indication that in the potential cycling synthesis only oxyhydroxide compounds of Fe(III) (amorphous or nanocrystalline) are obtained, which after the annealing are transformed in the $\alpha\text{-Fe}_2\text{O}_3$ phase. Nanocrystalline hematite films presenting an average crystallite size of ca. 36 nm were obtained.²⁵

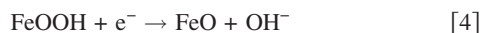
In order to study the film growth, the synthesis was followed by using an EQCM. Figure 1a shows the first voltammetric cycle of current density and mass change-potential curves obtained by the EQCM experiments with an Au electrode in the electrodeposition bath during the first potential cycle. In this cycle the electroreduction of H_2O_2 starts at around 0.0 V vs SMSE, but from -0.2 V the electrode shows a mass increase. The last is a consequence of the increase of the electrogenerated OH^- anion concentration in the vicinity of the electrode, which in turn increases the local pH and then the oxyhydroxide compounds of iron(III) precipitated onto the electrode according to the following reactions



With a global reaction



From -0.7 V the mass increase is stopped, probably due to a reduction of the film previously formed, through the reaction



In the reverse cycle, a slight mass decrease can be observed, probably due to the last reaction. In this potential range both reactions could be taking place, the film formation and the film reduction, for which mass variation is opposite; while the film formation increase the mass, the film reduction, decrease it, so the final mass

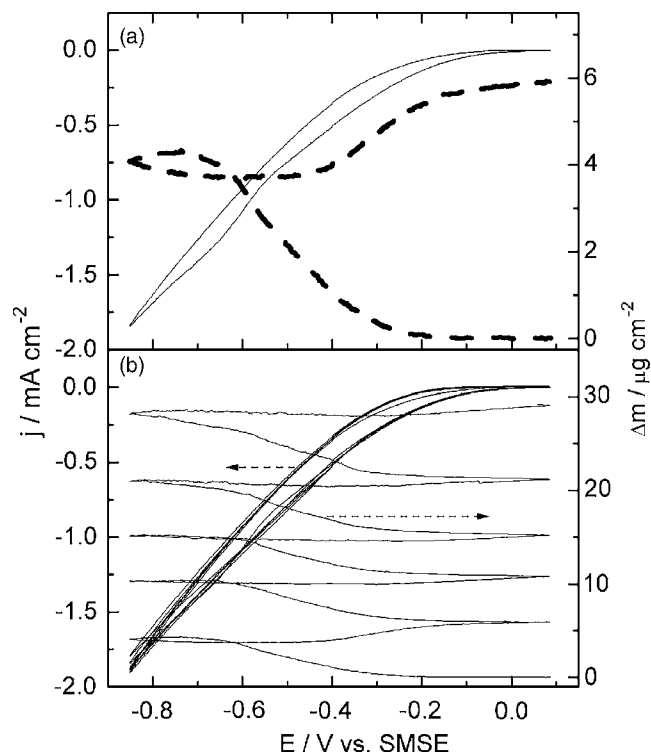


Figure 1. Cyclic voltammograms of an Au electrode and mass-potential curves in 5 mM FeCl_3 + 5 mM KF + 1 M H_2O_2 + 0.1 M KCl. Scan rate 0.02 V s^{-1} . (a) First voltammetric cycle. (b) First five voltammetric cycles.

variation could be null. From -0.4 V the mass increases again as a consequence of the electroformation of OH^- anion and that the reduction of the film is lower than the film formation at potentials more anodic than -0.5 V . The presence of a naked zone in the substrate is not discarded, so the film precipitation could be continuing in those zones. Figure 1b shows the behavior of the first five cycles; from the second cycle the mass increase observed in the reverse cycle is lower than in the first one, due to the complete covering of the gold substrate by the film. The electroformation of the oxyhydroxide compound film could be evaluated from the charge-mass plot showed in Fig. 2, which has been obtained by

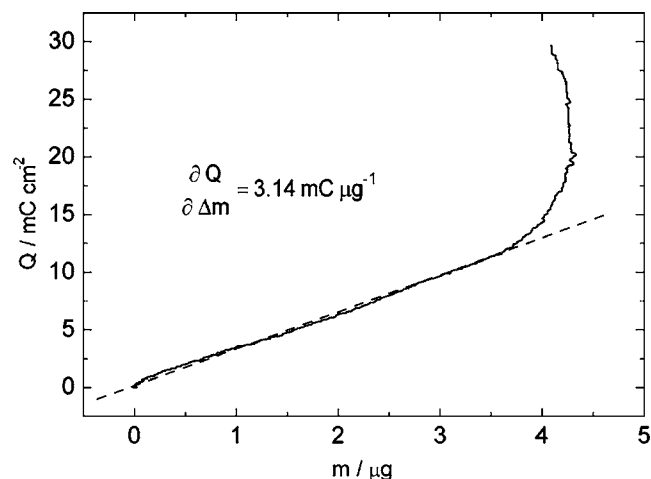


Figure 2. Charge-mass plot obtained by integration of the voltammogram of Fig. 1a.

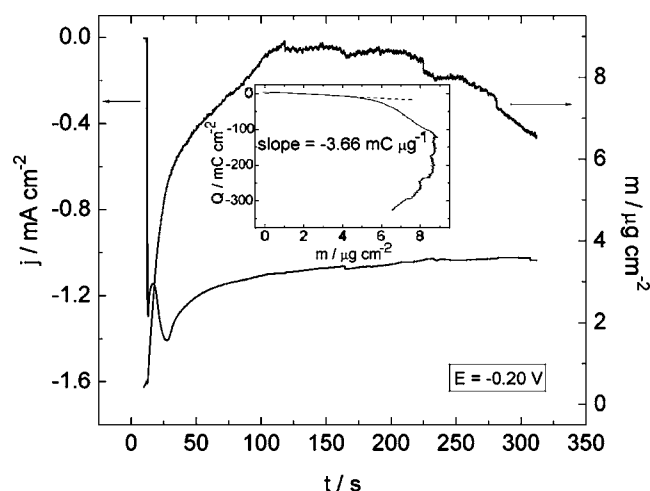


Figure 3. Current-time and mass-time curves obtained during the potentiostatic growth of $\alpha\text{-Fe}_2\text{O}_3$ in the same electrolyte as in Fig. 1. Electrodeposition potential $E = -0.20$ V. The inset shows the related charge-mass plot and the corresponding slope value is indicated.

integration of the voltammogram of Fig. 1a. The slope of the initial zone is $3.14 \text{ mC } \mu\text{g}^{-1}$, which is close to the theoretical charge mass ratio of $3.26 \text{ mC } \mu\text{g}^{-1}$ for Reaction 3.

Moreover, the same experience has been carried out in the potentiostatic mode, imposing a potential (E) at which the hydrogen peroxide is reduced (three different electrodeposition potentials have been assayed, i.e., $E = -0.10$, -0.15 , and -0.20 V). For $E = -0.10$ and $E = -0.15$ V, it was observed that the mass initially increases but after ca. 1 min it remains almost constant (results not shown), but for $E = -0.20$ V the mass increases until reaching a maximum at 2 min, after which, the mass decreases (see Fig. 3). The initial mass increase can be due to the reduction of hydrogen peroxide to hydroxyl anion, with the subsequent precipitation of iron(III) oxyhydroxide compound, according to Eq. 1-3. To confirm this phenomenology, charge-mass plots have been designed for each of the examined electrodeposition potential experiments, and the one corresponding to $E = -0.20$ V is shown as an inset in Fig. 3. The slopes of the initial state (first 30 s) were 3.06, 3.26, and $3.66 \text{ mC } \mu\text{g}^{-1}$ for $E = -0.10$, -0.15 , and -0.20 V, respectively. These values are close to the expected value according to Reaction 3. At longer times the slope is greater than this value due to the reduction of the film (as indicated by Eq. 4) which diminishes the mass. So at longer times the mass variation is a combination of the mass increase and mass decrease due to the film formation and film reduction, respectively. At more cathodic potentials, the slope is greater than the one obtained at -0.10 V, because the mass is lower than expected due to the film reduction taking place at the FTO/oxide interface, and the cathodic electrical charge is enhanced by the film reduction as well. In the case where the potential value was -0.20 V, a maximum in the $\Delta\text{mass}/\text{time}$ plot is observed. This is consistent with the idea that after Δmass reaches a stationary value, at this potential the rate of the reduction process (diminution of mass) is greater than those associated with the OH^- ions that are generated to precipitate the iron oxyhydroxide compound (increase of mass).

Semiconductor properties of the $\alpha\text{-Fe}_2\text{O}_3$ thin films.— In Fig. 4, current density vs potential curves for an $\alpha\text{-Fe}_2\text{O}_3$ electrodeposited and annealed thin-film electrode are shown under illumination of light and in the dark in 0.1 M NaOH + 0.05 M KI solution at pH 13. The increase in current observed upon illumination of the electrode confirmed the $\alpha\text{-Fe}_2\text{O}_3$ film to be photoelectrochemically active. The inset of Fig. 4 shows the steady-state photocurrent density (the difference $j_{\text{light}} - j_{\text{dark}}$ is just the photocurrent density j_{ph}). The

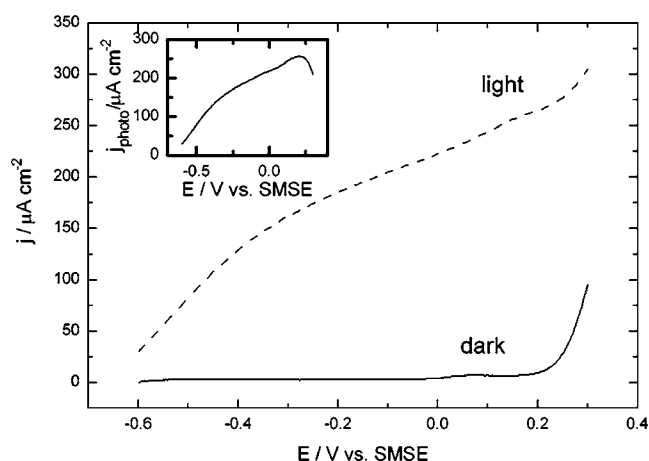


Figure 4. Current density-potential (j - E) characteristics of an annealed $\alpha\text{-Fe}_2\text{O}_3$ /FTO electrode in 0.1 M NaOH + 0.05 M KI (scan rate 0.02 V s^{-1}) in the dark (—) and under illumination (---) as indicated. (Inset) Photocurrent-potential curve for the annealed $\alpha\text{-Fe}_2\text{O}_3$ /FTO electrode in 0.1 M NaOH + 0.05 M KI.

onset of the photocurrent (that is, the potential at which the photocurrent starts to flow, E_{onset}) is located at around -0.65 V (the photocurrent onset gives approximately the position of the flatband potential, V_{FB} , *vide infra*). The anodic character of the photocurrent indicates that the film exhibits photoactivity with n-type behavior. The main defect in hematite is oxygen vacancies, which are responsible for the n-type behavior by donated electrons to the conduction band.¹¹ Moreover, it has been stated that high annealing temperatures enhance the oxygen vacancy concentration.¹¹ From the onset potential and up to 0.2 V, the photocurrent increases with a constant and negligible dark current, and then, for higher applied bias, both photo- and dark currents increase. At more anodic potentials than 0.2 V oxidation of water at the substrate FTO/electrolyte interface can take place, which must be responsible for the increase in the dark current at higher potentials.⁹ However, scanning the electrode potential cathodically, several hundred millivolts more negative than the photocurrent onset, an increase in the dark current can be observed, probably due to reduction of the photoelectrode (cathodic decomposition) and/or reduction of water.^{9,11} Moreover, the inset of Fig. 4 shows that the photocurrent exhibits a maximum located at ca. 0.2 V. A similar behavior has been reported in the literature for the $\alpha\text{-Fe}_2\text{O}_3/\text{KI}$ and $\alpha\text{-Fe}_2\text{O}_3\text{-TiO}_2/\text{H}_2\text{SO}_4$ systems.^{5,28} One possible explanation of this phenomenon has been suggested by Björkstén et al.,⁵ and can be related to the presence of surface states, whose energetic position can be estimated to be centered at ca. 0.15 V. So, when the semiconductor electrode is polarized anodic with respect to this potential, the surface states are empty and could become efficient recombination centers via trapping of conduction-band electrons.⁵

In a strict sense, due to the nanocrystalline morphology of the films, the simple Mott-Schottky equation may not be applicable.⁵ However, in a first approximation this type of analysis can be applied to nanostructured systems. In fact, examples of this approach to characterize nanostructured semiconductor thin films can be encountered in the literature.^{8,19} The characteristic Mott-Schottky plots for an $\alpha\text{-Fe}_2\text{O}_3$ electrode in 0.1 M NaOH solution at pH 13 measured at various ac frequencies (0.1, 0.5, and 1.0 kHz) are shown in Fig. 5. The measurements were carried out at different ac frequencies in order to check whether there is a large frequency dependency on the calculated doping and flatband potential. In Fig. 5, straight-line portions at the more anodic potentials are observed at all the studied ac frequencies. The linear C^{-2} vs E zero-voltage extrapolation resulted in a mean value of -1.06 V for all the three measured ac frequencies, exhibiting a very low dispersion. Hence,

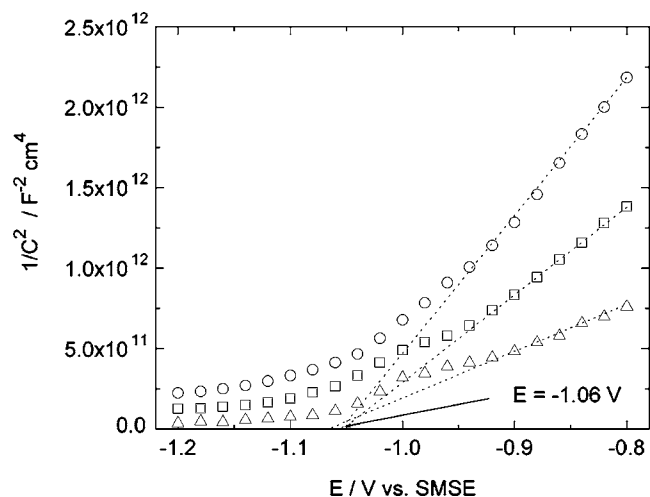


Figure 5. Mott-Schottky plot for an annealed $\alpha\text{-Fe}_2\text{O}_3/\text{FTO}$ film measured at 0.1 kHz (Δ), 0.5 (\square) and 1 kHz (\circ) under dark conditions. Electrolyte: solution 0.1 M NaOH, pH 13. The value of the intercept of the linear fitting with the abscissa is indicated as well.

after subtraction of the thermal contribution kT/e for $T = 298$ K, a flatband potential of -1.08 V was found. This value of flatband potential is consistent with results reported earlier for $\alpha\text{-Fe}_2\text{O}_3$ semiconductors (-1.050 V in 0.01 M NaOH, pH 12⁵). The onset potential E_{onset} of -0.65 V and the flatband potential E_{FB} of -1.08 V did not match very well in this case. The onset potential obtained from steady-state photocurrent experiments, in general gives (in n-type semiconductors) values which are several hundred millivolts more anodic than the flatband potential obtained by other methods (i.e., transient photocurrent method).¹ This could be due to the availability of surface-forbidden electrons at the surface to react with highly active intermediates, causing a decrease in the steady-state photocurrent at low band bending in the presence of redox species exhibiting slow charge-transfer kinetics.¹ The donor density N_D was calculated from the slope of the plots of Fig. 5 using the Mott-Schottky equation.²⁹ A dielectric constant of 12.5 was used for $\alpha\text{-Fe}_2\text{O}_3$.³⁰ Because the slopes of these plots changed with the ac frequency, the donor density also changed and can be attributed to numerous causes such as, among others, surface states.⁸ So, such donor density can be termed as the apparent donor density, as the donor density itself should not be frequency dependent.⁸ In the present case, the frequency dependence of the apparent donor density of $\alpha\text{-Fe}_2\text{O}_3$ was relatively small, 4.1 and $1.26 \times 10^{19} \text{ cm}^{-3}$ at the ac frequencies of 0.1 and 1 kHz, respectively. The higher apparent donor density at the lower ac frequency can be attributed to the fact that at lower frequency, some contribution coming from the surface states may be present.⁸ In order to compare this with results presented in the literature, the apparent donor density at 1 kHz of the $\alpha\text{-Fe}_2\text{O}_3$ thin films, $N_D = 1.26 \times 10^{19} \text{ cm}^{-3}$, are further considered. This donor density value is higher than the ones presented by hematite films obtained by thermal growth and single-crystal $\alpha\text{-Fe}_2\text{O}_3$ ($10^{17}\text{--}10^{18} \text{ cm}^{-3}$).³¹ This donor density value is lower than the corresponding donor density exhibited by anodic oxide thin films ($10^{20}\text{--}10^{21} \text{ cm}^{-3}$).³¹ However, this donor density is similar to that exhibited by $\alpha\text{-Fe}_2\text{O}_3$ thin films obtained by a sol-gel procedure, i.e., $5.64 \times 10^{19} \text{ cm}^{-3}$.¹⁸ It must be taken into account that measurement of N_D is complicated by partial compensation in the oxide.³⁰ Moreover, the donor densities reported do not correspond to impurity concentrations but rather only approximate the nonstoichiometry (Fe^{+2}) of the space-charge region.³⁰ A high donor density reduces the resistivity of the film, resulting in the increase in incident photon-to-current efficiency of $\alpha\text{-Fe}_2\text{O}_3$ photoelectrochemical cells in the visible as well as in the UV range.¹⁸

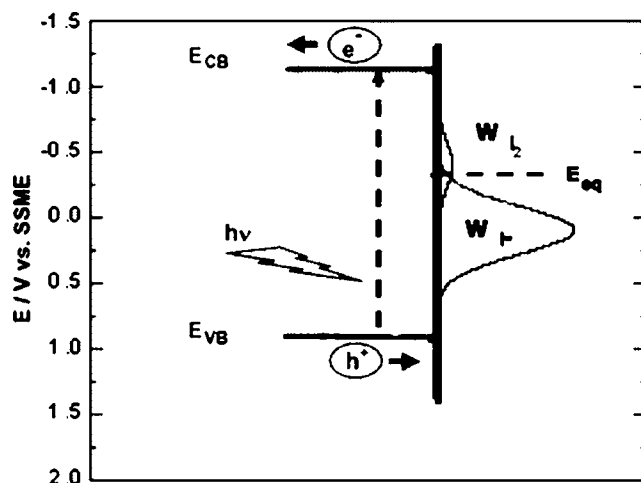
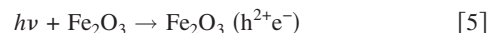


Figure 6. Energy-band diagram for a $\alpha\text{-Fe}_2\text{O}_3/\text{FTO}/\text{electrolyte}$ interface at pH 13. Schematic representation of the different reaction pathways for the photogenerated electron-hole pair for a n-type $\alpha\text{-Fe}_2\text{O}_3$.

The photocurrent measured with a semiconductor electrode depends on the dynamics of photogenerated charge carriers and on the kinetics at the nanostructured semiconductor electrode-electrolyte interface.¹⁹ In order to assess the dynamics of photogenerated charge carriers, the energy-level diagram shown in Fig. 6 (on the electrochemical scale vs SMSE) for the nanostructured $\alpha\text{-Fe}_2\text{O}_3/\text{electrolyte}$ liquid junction was constructed. The various energy levels shown in this diagram were obtained as follows. The position of the conduction band edge (E_{CB}) for hematite was calculated from the flatband potential value obtained above, and by assuming that E_{C} lays at 0.1 eV above the Fermi level, we get $E_{\text{CB}} = -1.18$ V. Because the bandgap energy obtained for this electrodeposited and annealed $\alpha\text{-Fe}_2\text{O}_3$ thin film was 2.0 eV,²⁵ the valence band-edge level E_{VB} was taken at 0.82 V. Moreover, the redox potential energy level ($E = -0.38$ V) as well as the Gaussian energy distribution function of electron acceptor and donors levels in solution of I_2/I^- are also depicted. Photoexcitation produces electron-hole pairs in the iron oxide film (see Fig. 6)



The mechanism of charge separation in a nanocrystalline film is quite different from that in a conventional photoelectrochemical cell.³² In fact, charge separation occurs not by a space-charge layer (there is likely no band bending) but rather by differing rates of electron and hole transfer into solution.^{18,32} The transport of charge carriers is better described by a diffusion process.³³ After photoexcitation the following steps take place: (i) transfer of a hole over the nanostructured semiconductor electrode-electrolyte interface (NSEI), (ii) a hole-hole acceptor reaction in the electrolyte at the NSEI, oxidation step, i.e., I^- to I_2 , (iii) electron transport of electrons through the semiconductor nanoparticle iron oxide film, and (iv) transport of the electron through the outer circuit to the counter electrode. So, the reaction described in step (ii) is responsible for the anodic character of the photocurrent observed in Fig. 4. While photoexcitation has been proven to be extremely fast, the reaction over the NSEI [step (ii)] depends on the interfacial rates of reaction between the charge carrier passing over the NSEI (hole in our case) and accepting species in the electrolyte. For instance, in an n-type nanostructure, an efficient hole-accepting species in solution can accelerate the interfacial reaction. Moreover, fast hole kinetics at the NSEI is of importance to prevent recombination of the photogenerated charges and consequently enhancing the incident photon-to-current efficiency of photoelectrochemical cells. In this sense, iodide is a well-known hole scavenger.¹¹

Conclusion

The voltammetric analysis allows for studying the formation of oxyhydroxide iron compounds, which after an annealing treatment takes to the formation of hematite thin films. The potential cycling procedure permits film growth because it maintains a higher hydroxyl concentration in the electrode interface, while this behavior is not observed when the synthesis is performed by a potentiostatic procedure. The EQCM study showed that the resulting film could be a complex mixture of hydrated oxyhydroxide iron(III) compounds. Photoelectrochemical results in liquid junction with 0.1 M NaOH + 0.05 M KI electrolyte at pH 13 showed an n-type character of the α -Fe₂O₃ thin films, and a flatband potential of -1.08 V vs SMSE (pH 13) and a apparent donor density of 1.26×10^{19} cm⁻³ were found from the Mott-Schottky plots at the ac frequency of 1 kHz.

Acknowledgments

This work has been supported by FONDECYT (Chile) project no. 1040658. E.A.D. thanks CSIC (Universidad de la República) and PEDECIBA-FISICA, Uruguay.

PEDECIBA-Física assisted in meeting the publication costs of this article.

References

- M. Anderman and J. H. Kennedy, *J. Electrochem. Soc.*, **131**, 21 (1984).
- J. H. Kennedy and K. W. Frese, Jr., *J. Electrochem. Soc.*, **125**, 709 (1978).
- J. H. Kennedy and M. J. Anderman, *J. Electrochem. Soc.*, **130**, 848 (1983).
- S. Mohanty and J. Ghose, *J. Phys. Chem. Solids*, **53**, 81 (1992).
- U. Björkstén, J. Moser, and M. Grätzel, *Chem. Mater.*, **6**, 858 (1994).
- W. B. Ingler, Jr., and S. U. M. Khan, *Int. J. Hydrogen Energy*, **30**, 821 (2005).
- W. B. Ingler, Jr., and S. U. M. Khan, *Electrochem. Solid-State Lett.*, **9**, G144 (2006).
- S. U. M. Khan and J. Akikusa, *J. Phys. Chem. B*, **103**, 7184 (1999).
- N. Beermann, L. Vayssieres, S.-E. Lindquist, and A. Hagfeldt, *J. Electrochem. Soc.*, **147**, 2456 (2000).
- A. Kay, I. Cesar, and M. Grätzel, *J. Am. Chem. Soc.*, **128**, 15714 (2006).
- T. Lindgren, H. Wang, N. Beermann, L. Vayssieres, A. Hagfeldt, and S.-E. Lindquist, *Sol. Energy Mater. Sol. Cells*, **71**, 231 (2002), and references therein.
- N. J. Cherepy, D. B. Liston, J. A. Lovejoy, H. Deng, and J. Z. Zhang, *J. Phys. Chem. B*, **102**, 770 (1998).
- F. Sánchez-Bajo, A. L. Ortiz, and F. L. Cumbreira, *Acta Mater.*, **54**, 1 (2006).
- J. D. Desai, H. M. Pathan, S.-K. Min, K.-D. Jung, and O. S. Joo, *Appl. Surf. Sci.*, **252**, 1870 (2005).
- H. E. Prakasam, O. K. Varghese, M. Paulose, G. K. Mor, and C. A. Grimes, *Nanotechnology*, **17**, 4285 (2006).
- Z. R. Dai, Z. W. Pan, and Z. L. Wang, *Adv. Funct. Mater.*, **13**, 9 (2003), and references therein.
- A. Duret and M. Grätzel, *J. Phys. Chem. B*, **109**, 17184 (2005).
- H. Miyake and H. Kozuka, *J. Phys. Chem. B*, **109**, 17951 (2005).
- Electrochemistry of Nanomaterials*, G. Hodes, Editor, Wiley-VCH Verlag GmbH, Weinheim (2001).
- S. T. Chang, I. C. Leu, and M. H. Hon, *Electrochem. Solid-State Lett.*, **5**, C71 (2002).
- T. Pauporté and D. Lincot, *Appl. Phys. Lett.*, **75**, 3817 (1999).
- D. Lincot, *Thin Solid Films*, **487**, 40 (2005).
- L. Martinez, D. Leinen, F. Martín, M. Gabas, J. R. Ramos-Barrado, E. Quagliata, and E. A. Dalchiele, *J. Electrochem. Soc.*, **154**, D126 (2007).
- G. Zotti, G. Schiavon, S. Zecchin, and U. Casellato, *J. Electrochem. Soc.*, **145**, 385 (1998).
- R. Schreblor, K. Bello, F. Vera, P. Cury, E. Muñoz, R. del Río, H. Gómez Meier, R. Córdova, and E. A. Dalchiele, *Electrochem. Solid-State Lett.*, **9**, C110 (2006).
- S. Langerock and L. Heerman, *J. Electrochem. Soc.*, **151**, C155 (2004), and references therein.
- Y. W. Chen, D. Cahen, R. Noufi, and J. A. Turner, *Sol. Cells*, **14**, 109 (1985).
- H. Kim, N. Hara, and K. Sugimoto, *J. Electrochem. Soc.*, **146**, 955 (1999).
- A. J. Bard and L. R. Faulkner, *Electrochemical Methods, Fundamental and Applications*, John Wiley & Sons, Inc., New York (1980).
- Handbook of Chemistry and Physics*, 74th ed., D. R. Lide, Editor, CRC, Boca Raton, FL (1994).
- S. M. Wilhelm, K. S. Yun, L. W. Ballenger, and N. J. Hackerman, *J. Electrochem. Soc.*, **126**, 419 (1979), and references therein.
- G. Hodes, I. D. J. Howell, and L. M. Peter, *J. Electrochem. Soc.*, **139**, 3136 (1992).
- S. Södergren, A. Hagfeldt, J. Olsson, and S.-E. Lindquist, *J. Phys. Chem.*, **98**, 5552 (1994).